pH-Based Cancer Detection by Graphene Quantum Dots

Veronica Lyle

Background

1.1 Defining Quantum Dots and their Relevant Properties

Quantum Dots are nanoscale semiconductor particles best known for their unique optical and electronic properties, in particular their tunable fluorescence[1]. These properties, which differ quantum dots from bulk (larger than nanoscale) semiconductors made of identical materials, are exhibited due to elements of quantum mechanics which apply to molecules confined to the nanoscale (less than 500nm in at least one dimension)[2]. Quantum Dots are confined to the nanoscale in three dimensions—length, width, and height—and so are considered zero-dimensional particles[1].

The phenomenon of tunable fluorescence in quantum dots is best explained by a combination of the properties of semiconductors and the classic 'particle in a box' model touted in Quantum Mechanics[2,3]. The electric behavior of semiconductors lies between those of conductors and insulators, which are characterized by partially-filled and occupied quantum states respectively[2]. The partially-filled orbitals of conductors translates to large quantities of delocalized electrons, which can travel easily throughout the material. Alternatively, insulators' occupied quantum states block delocalized movement, as per the Pauli Exclusion Principle, only one charge carrier can occupy a given state at a time. Insulators are not completely immovable. Partially occupied states can be seen in few locations where electrons have been sufficiently excited to cross what is known as the band gap, the energy difference between the highest filled orbital (valence band) and the lowest unoccupied orbital (conductance band). In insulators, this gap is often too large to overcome, whereas in conductors, the gap is functionally nonexistent. Semiconductors exist in the middle—the bandgap is significant, but sufficiently small, usually approximately 1.5eV, to be overcome. When electrons in the valence band are struck by photons, they transfer to the conductance band[4]. Eventually, they return to the valence band, at which time they release a photon of a wavelength corresponding to the energy of the band gap. For a standard sized semiconductor, this band gap is largely influenced by the crystal lattice structure of the material used, and thus relatively restricted. Small adjustments can only be made by doping semiconductors with other compounds[4].

Quantum Dots, as semiconductor particles, exhibit these same characteristics of valence and conductance bands and photon emission. However, due to their aforementioned nanoscale dimensions, quantum dots experience a property known as quantum confinement. Quantum confinement occurs when a semiconductor is smaller than two times the distance between a conductance band electron and its corresponding hole in

the valence band, also known as the exciton Bohr radius. At this scale, the excitons are effectively squeezed, which alters the energetic size of the band gap, and subsequently the wavelength of the emitted photon[5]. This adjustment can be calculated by equations resulting from the three-dimensional particle in a box model[3].

For this model, suppose a one-dimensional system, in which a particle exists in a space x between 0 and L where the potential is zero (no forces acting), with infinite potential on either side of this space. This can be modeled by equation 1[3].

$$V(x) = \begin{cases} 0, 0 < x < L \\ \infty, \text{otherwise} \end{cases} \qquad (1)$$

The behavior of the particle inside this space can be modelled by a wave function, which gives a description of the particle's momentum, position, and energy. This function can be derived from the free particle Schrödinger equation (see equation 2) for the system, as there are no forces acting on the particle in the space[3].

$$\psi(x, t) = [A\sin(kx) + B\cos(kx)]e^{-i\omega t} \qquad (2)$$

The energies of the corresponding permitted wavenumbers derived from this relationship may be written as the following:

$$E_n = \frac{n^2 h^2}{8mL^2} \qquad (3)$$

with n signifying the quantum number of the particle, h signifying Planck's constant, m signifying the mass of the particle, and L still signifying the length of the space. This model can be adapted for quantum dots to represent a particle confined in three dimensions, resulting in the equation of Brus, named for Louis Brus, who developed the technique[6]. The equation of Brus can be used to describe the energy change of the band gap ($\Delta E(r)$) resulting from adjustment of the particle's radius r. The equation is represented by the addition of the original band gap energy (E_{gap}) and the three-dimensional energy equation resulting from the particle in a box model shown in equation 4:

$$\Delta E(r) = E_{gap} + \left(\frac{h^2}{8r^2}\right)\left(\frac{1}{m_e^*} + \frac{1}{m_h^*}\right) \qquad (4)$$

with m_e^* signifying the electron's effective mass and m_h^* signifying the effective mass of the hole[11]. Using experimental data, this equation, in conjunction with the relationship relating energy to the wavelength (λ) of emitted light $E=hc/\lambda$, can be used to determine the new expected wavelength of the quantum dot's fluorescence resulting from a change

in radius[1]. The relationship derived between wavelength and particle radius results in one of the quantum dots' most unique properties—as the radius of the particle decreases, so too does the wavelength of the fluorescence. This relationship is the root of quantum dots' 'tunable' fluorescence[13]. While other properties of a quantum dot influence wavelength, including composition (including doping), shape and structure, the relationships corresponding to these properties are much more complex[7].

1.2 Graphene Quantum Dots for Biological Applications

The tunable fluorescence of quantum dots is especially attractive for biological applications, in particular fluorescence imaging. Commonly used organic dyes, while effective, are typically confined to a single color and degrade quickly, whereas quantum dots are not only tunable, but also significantly brighter and more stable[8].

An unfortunate drawback of many quantum dots for biological applications, however, relates to their toxicity. Quantum dots are often composed of toxic materials, such as the heavy metals cadmium and lead[9]. For that reason, carbon based quantum dots, most often graphene quantum dots (GQDs), are attractive due to their low toxicity, high biocompatibility and chemical stability[8]. The spectra of these quantum dots can vary from the ultraviolet (UV) to the infrared (IR) range, and are typically easily dispersed in aqueous solutions. Additionally, graphene quantum dots will often respond to specific environments, altering their fluorescence by way of intensity or wavelength. This property can be utilized as a biosensing mechanism if the specific species of quantum dot is reactive to a given chemical marker. Successful applications in drug/gene delivery, bioimaging, and biosensing, effectively enhancing treatment efficacy as a remarkably noninvasive delivery method, have been developed by many research groups[10-13]. Despite their ability to fluoresce between the UV and IR range, depending on composition, usable wavelength ranges for biological applications are narrow. Detection of any fluorescent tag, especially *in vivo,* is challenged by high autofluorescence background emission from the biological tissue spanning the majority of the UV and visible range, making visible fluorescence primarily suitable for *in vitro* applications[14]. Similarly, a narrow range in the nearinfrared region (NIR) centered at 950nm is ideal for any *in vivo* imaging applications due to low levels of autofluorescence in that range[15-16]. As a result, NIR-emissive GQDs are ideal candidates for bioimaging and biosensing applications in full-body small animal imaging, drug tracking in animal models, and potentially low depth imaging in human tissues[14].

1.3 The pH of Cancer

pH, a value determined by the concentration of hydrogen ions in solution, is one of the most tightly regulated variable is human physiology, as even small alterations in pH can potentially wreak havoc on otherwise healthy tissues due to the high sensitivity of many biological molecules' configuration to pH[17]. Cancer cells are not exempt from this tight regulation. However, cancerous pH, intracellular and extracellular, often has different set points from the healthy counterpart[18]. A large culprit for this change is due to cancer cells unique position of having high energy requirements, due to rapid proliferation, while also often being poorly perfused due to the aforementioned rapid growth, which is too rapid for blood vessels to be incorporated into the masses, or tumors. This energy need, coupled with an inability to rapid receive oxygen, makes it impossible for these cells to utilize the oxygen requiring metabolic pathway oxidative phosphorylation, causing many cells to utilize the less efficient lactic acid pathway. The hydrogen ions produced from this process are expelled from the cell, raising the pH of the extracellular environment[19]. Hypoxia also triggers increased expression of some proteins, such as the membrane bound extracellular carbonic anhydrase (CA), which catalyzes the reaction of carbon dioxide to bicarbonate and hydrogen ions. Numerically, these differences result in a pH difference that is large enough to be significant, with healthy cells exhibiting an intracellular pH of 7.2, while cancerous cells have an intracellular pH of 7.3 to 7.6, and the extracellular pH of healthy and cancerous cells respectively is 7.35-7.45 and 6.4-7.0. These changes in control of intracellular and extracellular acidity has been connected to many of the hallmarks of cancer, including its progression, diffusion, resistance to therapies, and 'invisibility' to the immune system[19]. However, with the correct technology, this characteristic may be utilized as a tool rather than barrier to cancer treatment.

Procedure

2.1 GQD Synthesis

We used 4 different forms of graphene quantum dots, chosen for their fluorescence peaks in the visible and infrared range. We synthesized Aluminum- doped Reduced Graphene Oxide Quantum Dots (Al-RGQDs) from glucose and urea, Glucose Graphene Quantum Dots (GGQDs) by exposing glucose to ammonia and microwaves, and L-Glutamic Acid Graphene Quantum Dots (LGGQDs) by exposing L-glutamic acid to heat. Reduced Graphene Oxide Quantum Dots were synthesized by combining a 0.43mg/mL solution of reduced graphene oxide to 1.5mL of sodium hypochlorite for 48 hours, followed by 96 hours in a dialysis bag to remove unreacted acid, changing the water every 24 hours.

2.2 pH Adjustment

The amounts and concentrations of each sample used were 20mL of 0.4mg/mL RGQD, 5mL of 0.67mg/mL GGQDs, 5mL of 20.4mg/mL LGGQDs, and 5mL of 7.5mg/mL Al-RGQDs. We measured pH using the Hanna HI2210 pH Meter. For all samples, an initial pH was taken, without any acid or base added, and spectra were recorded at the initial pH. Only LGGQDs had an initial pH out of the targeted biological pH range of 6.00-8.00, at a pH of 3.20. In order to obtain stepwise readings in the desired pH range, we added small amounts of acid or base to each sample to change the pH at intervals of approximately 0.25. It was found that 0.6M HCl, diluted from 12M stock solution, and 0.6M NaOH, mixed from solid state, when added in 5µL portions to the RGQD solution, was an reasonable amount to reach the desired interval. Accordingly, for the other three samples, we mixed a 0.15M HCl and NaOH, due to their smaller volume, so 5µL amounts were still added to reach subsequent pHs. For each sample, we added the necessary acid or base, vortexed the solution using a fisher scientific digital vortex mixer for 20 seconds, and then the pH probe was placed in the sample for 5 minutes, until the pH reading had settled. If more acid or base was necessary to reach the target pH, we repeated the procedure. Once at the desired pH, we transferred 3mL of sample to a cuvette for imaging.

2.3 Imaging

Once placed in a cuvette, we recorded the sample's visible and infrared spectra. The visible spectra was taken using a Horiba Spectral Array which utilized a lamp for light exposure and the IHR 320 Syncerity for data collection. These devices were controlled and data saved using the program FluorEssence V3.8.Through this software, the excitation was set at a wavelength of 400nm for a range of 440 to 700nm, with a slit of 5nm, and gratings set at 1200 and 500. Integration time was 1 second.

We similarly attempted to take the IR spectra using the horiba apparatus, replacing the IHR 320 Syncerity with the IHR 320 Syncerity II. For RGQDs, we found that the lamp was insufficient to excite the sample enough to provide reliable spectra, and so instead we used an 808nm laser with the software AvaSoft 8. Via trial and error, the aforementioned concentrations were found to be sufficient to show peaks in the IR range of 840nm to 1115nm, with an integration time of 30 seconds. We repeated this 808nm method for IR spectra collection of GGQDs and Al-RGQDs. We used a 400nm laser and integration time

of 60 seconds for LGGQDs. We then converted the data from ASCII files to excel using Origin 2018b 64bit to allow for interpretation.

Once converted into Microsoft excel friendly format, we collected the visible and IR spectra for each sample were placed on a single graph, for a total of 9 spectra per graph from pH6.00-8.00 in intervals of approximately 0.25. We then color coded each spectra according to the classic order of red, orange, yellow, etcetera, ending with purple, for ease of visual interpretation.

Results

All materials were found to have spectra with peaks at consistent wavelengths regardless of pH. However, for each sample, alterations in the intensity were observed for each sample, which in some cases correlated to pH. RGQDs, GGQDs and LGGQDs showed correlation between pH and their visible spectra, but the infrared spectra of these three, while varying in intensity across different pH measurements, did not vary in any trackable way with respect to pH. GGQDs visible spectra's intensity increased with decreasing pH, while RGQDs and LGGQDs visible spectra's intensity increased with increasing pH. Both the Al-RGQD spectra correlated with pH. The visible Al-RGQD spectra increased intensity with decreasing pH, while the IR intensity increased with increasing pH. See the summary table of these results, and the graphs of the individual results below.

Intensity with Increasing pH	RGQDs	GGQDs	LGGQDs	Al-RGQDs
Visible	Increasing	Decreasing	Increasing	Decreasing
Infrared	No correlation	No correlation	No correlation	Increasing

Table 1: Summary of the correlation between pH and Intensity in the visible and infrared spectrum for each quantum dot type used

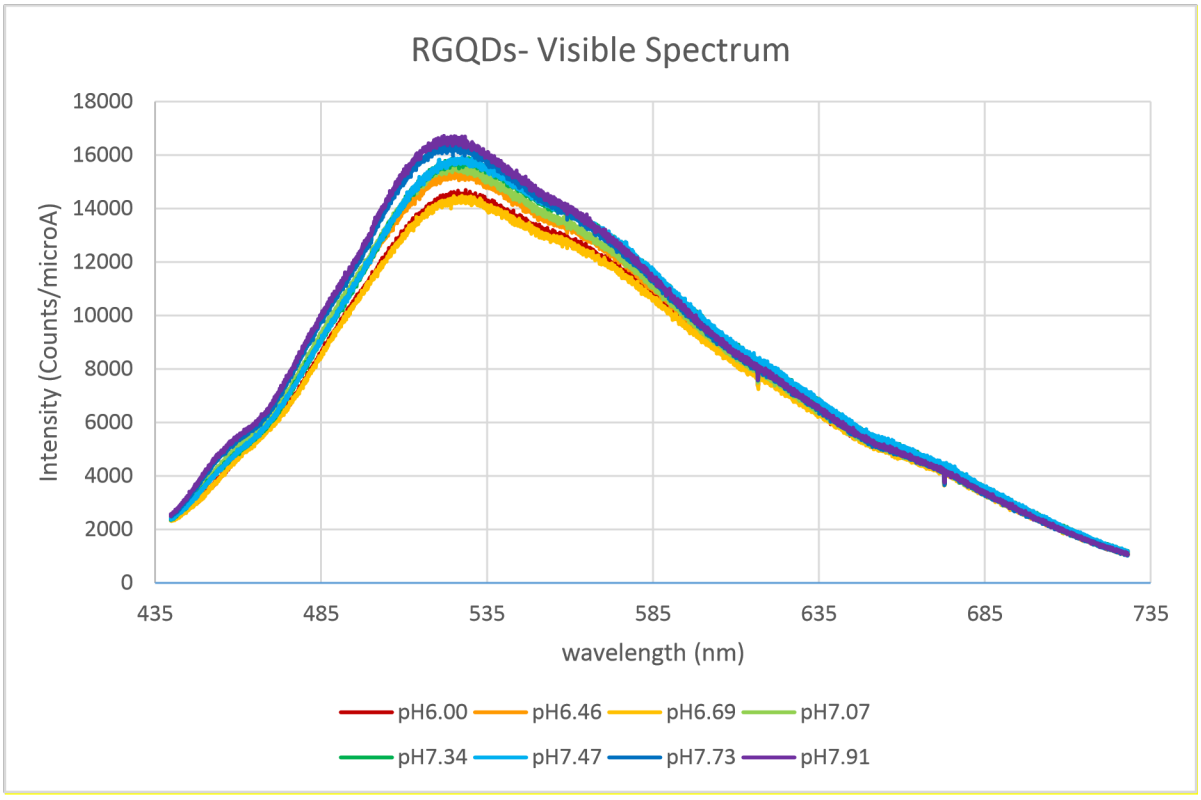

Figure 1: pH-varied emission spectra of RGQDs in the visible range

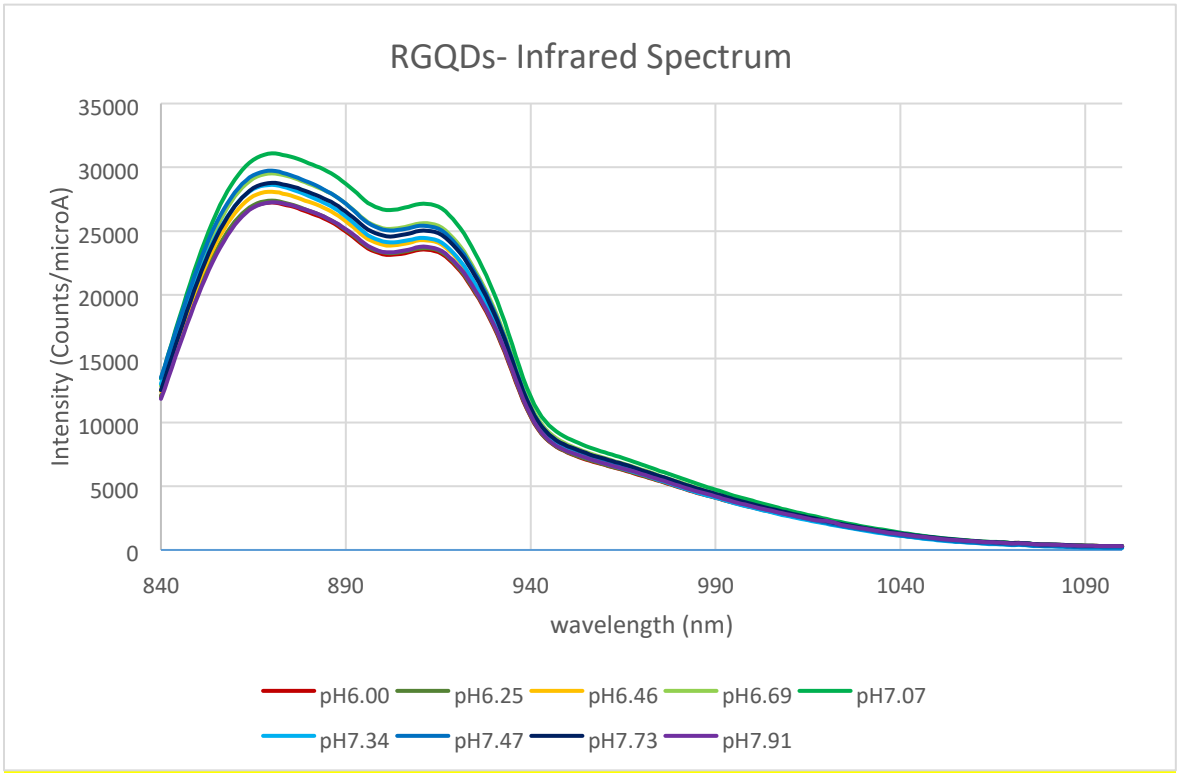

Figure 2: pH-varied emission spectra of RGQDs in the near infrared range

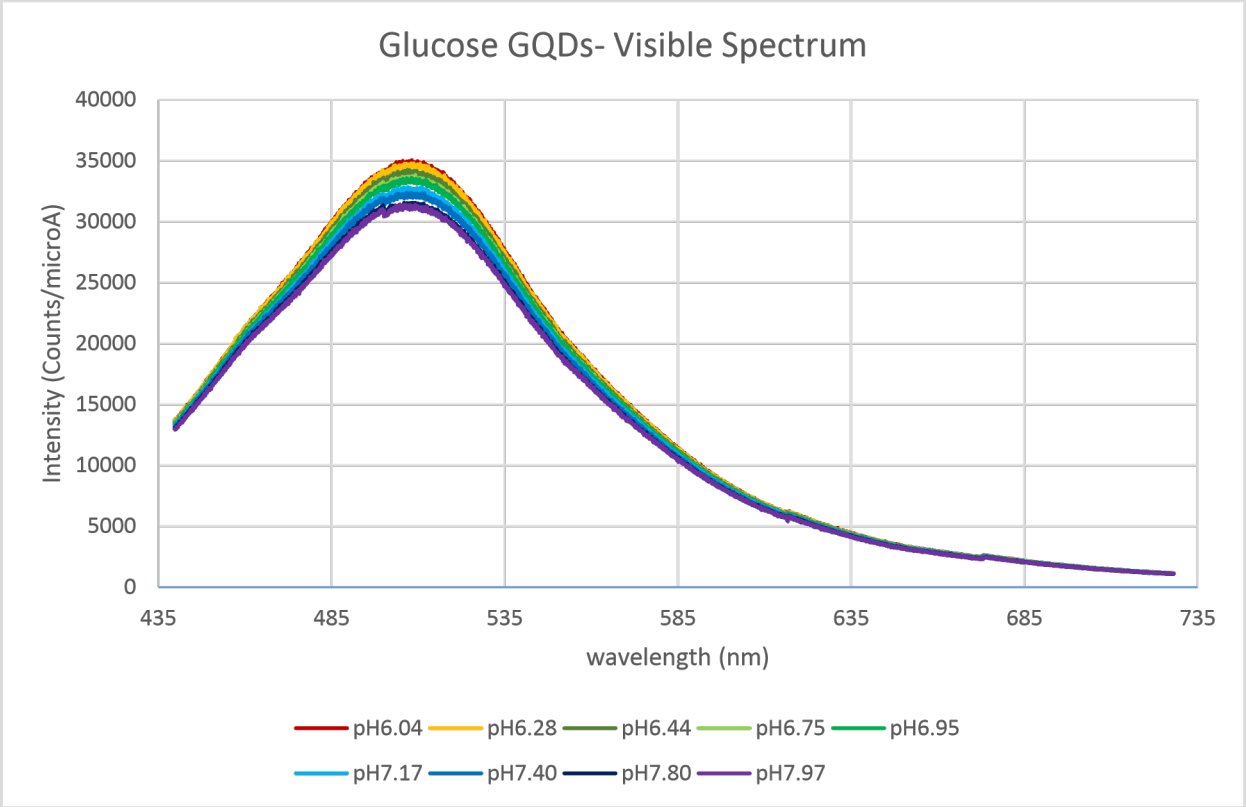

Figure 3: pH-varied emission spectra of GGQDs in the visible range

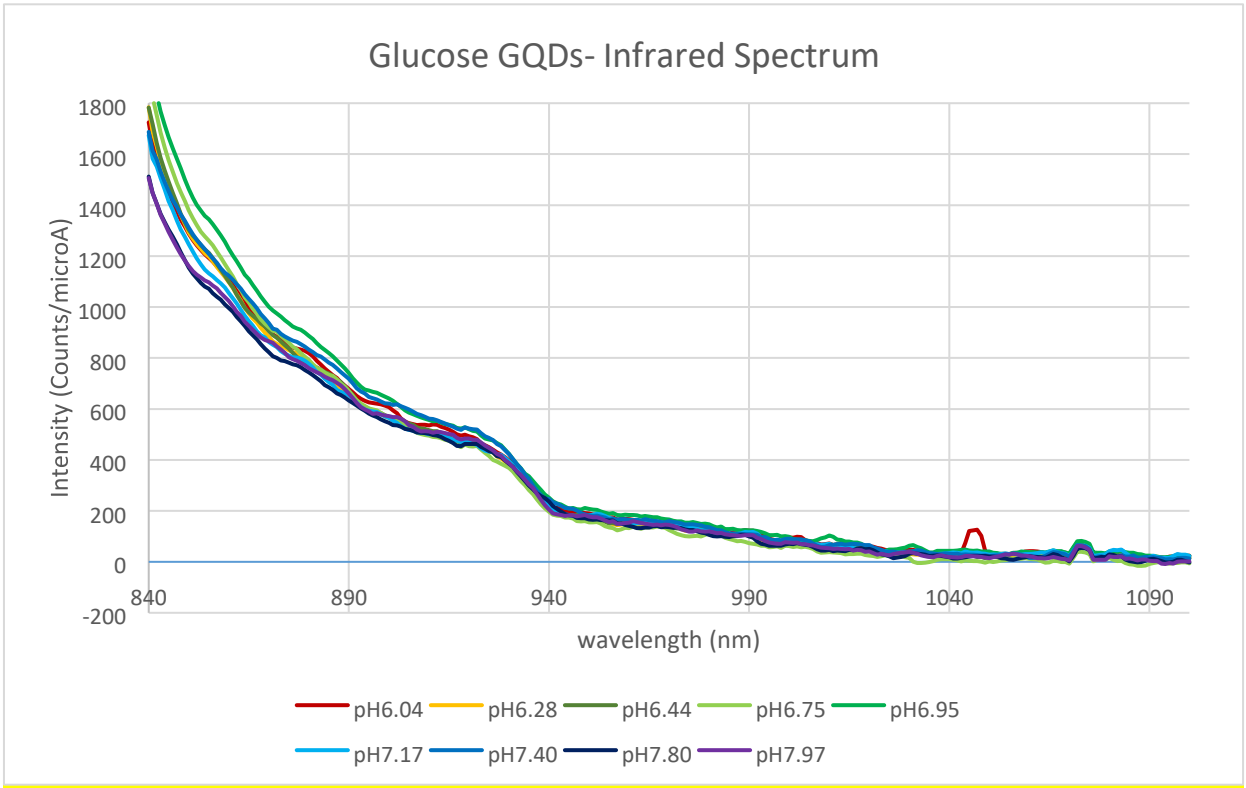

Figure 4: pH-varied emission spectra of GGQDs in the infrared range

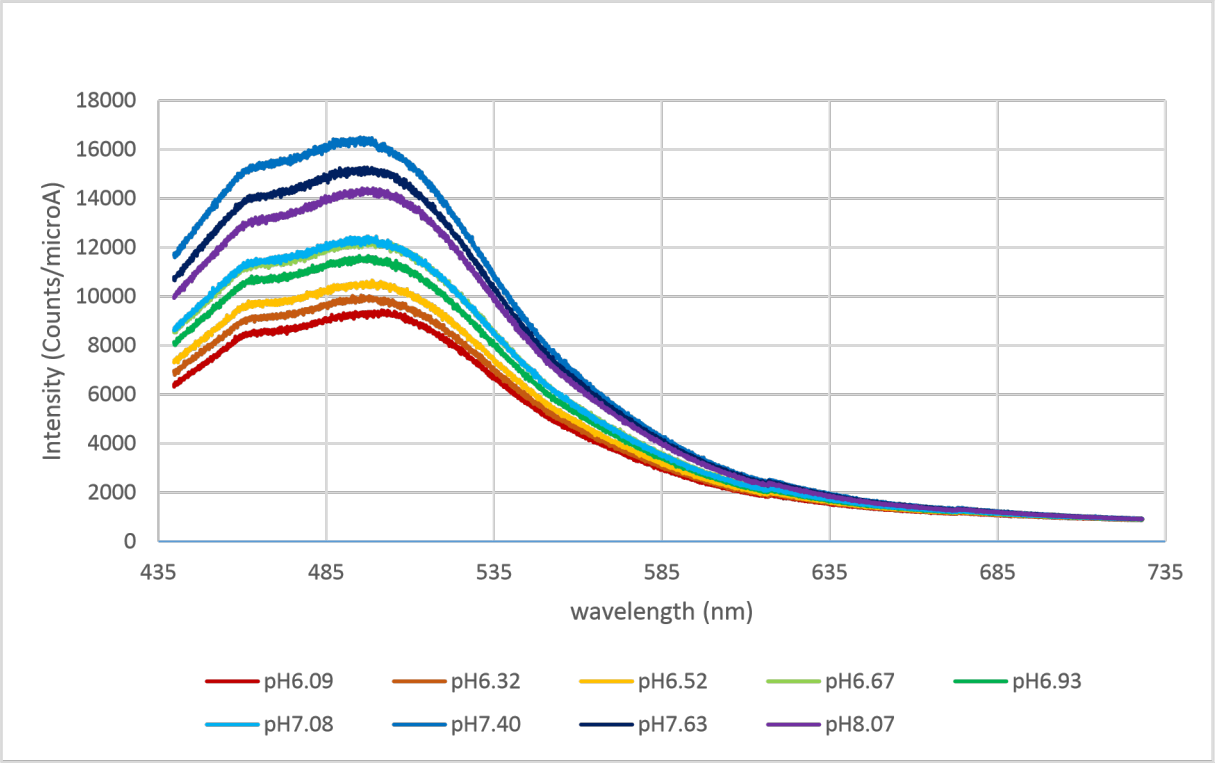

L-Glutamic GQDs- Visible Spectrum

Figure 5: pH-varied emission spectra of LGGQDs in the visible range

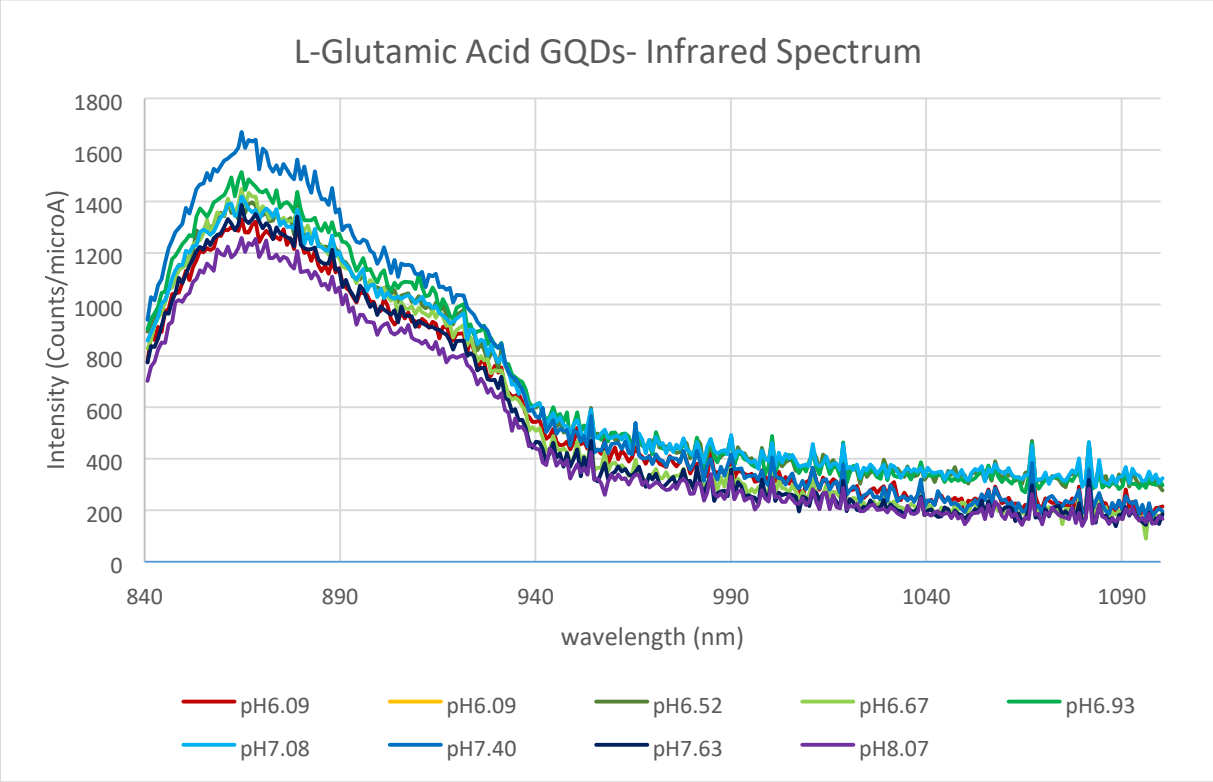

Figure 6: pH-varied emission spectra of LGGQDs in the infrared range

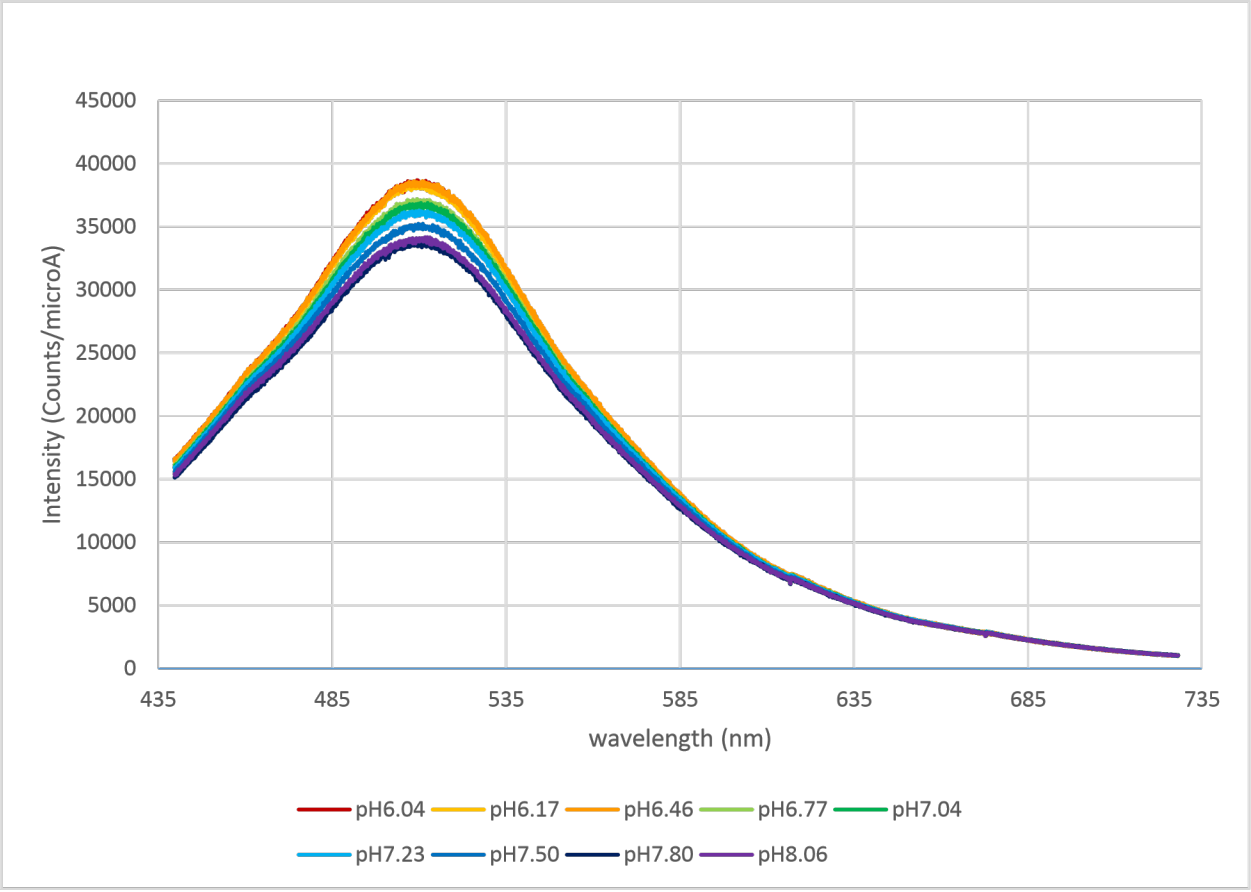

Figure 7: pH-varied emission spectra of Al-RGQDs in the visible range

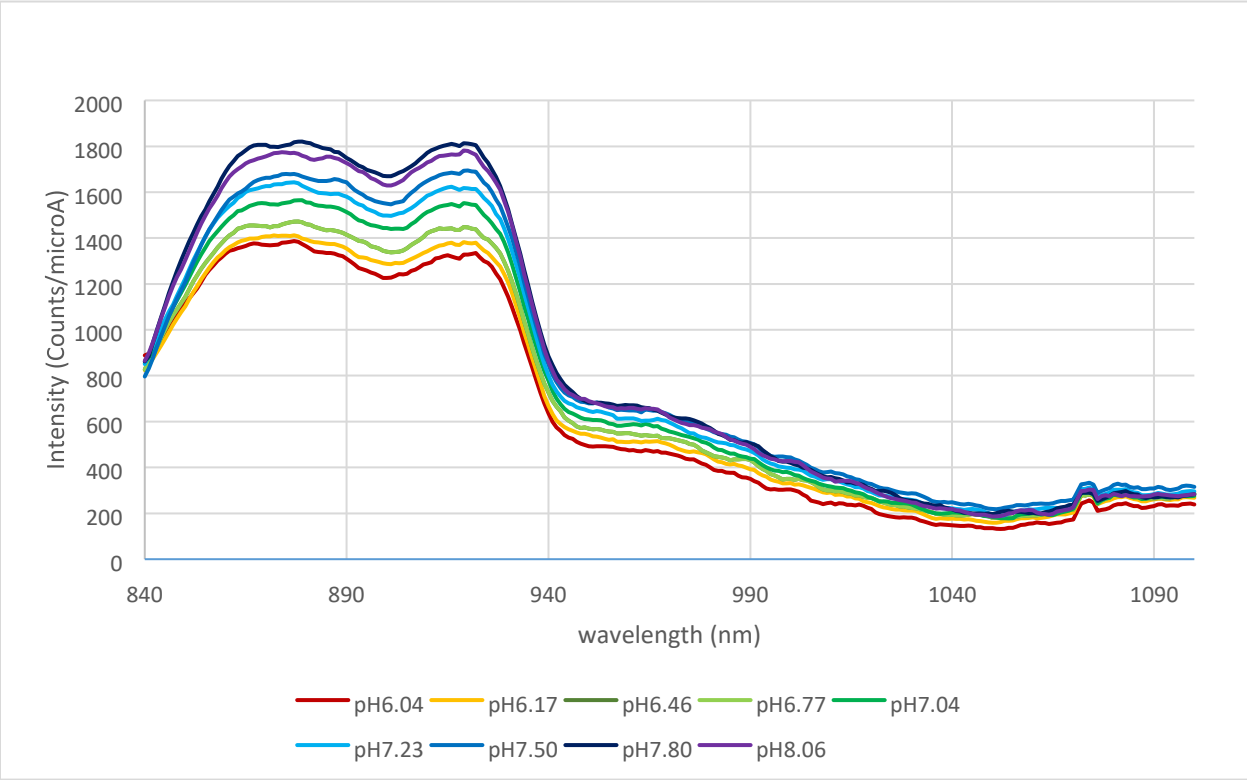

Figure 8: pH-varied emission spectra of Al-RGQDs in the infrared range

Conclusions

Of the 8 spectra collected, four, spanning three of the materials, show promise as potential methods for the detection of cancer through pH sensitivity. RGQDs showed no particular affinity for pH and fluorescence in either the visible or infrared range. Both LGGQDs and GGQDs showed correlation between intensity and pH in the visible range. LGGQD intensity increasing with pH up to a pH of 7.4, which is within an acceptable range for cancer detection considering healthy cellular environments reside at a minimum of 7.35, and cancerous much lower. GGQD intensity decreases with increasing pH across the full range tested. Al-RGQDs, however, showed by far the best results. Al-RGQD intensity not only decreased with intensity with increasing pH, but was the only one of the four tested which showed a strong correlation between pH and the spectra in the infrared range, with intensity increasing with pH across the tested range. These correlations can be definitively attributed to pH, as the only other factor changed between recordings was concentration at an overall increase of less than 2%, with pH readings taken in random order. These results indicate that GGQDs, LGGQDs, and Al-RGQDs should be further investigated in biological environments for their pH sensitivity in the visible spectra for future *in-vitro* imaging methods, and Al-RGQDs infrared spectra should similarly be investigated in the infrared range for future *in-vivo* pH detection methods.

References

1. Wang, Yilin, et al. “Simple Synthesis of Luminescent CdSe Quantum Dots from Ascorbic Acid and Selenium Dioxide.” Luminescence, vol. 30, no. 8, 2015, pp. 1375– 1379., https://doi.org/10.1002/bio.2909
2. Yu, Peter Y., and Manuel Cardona. Fundamentals of Semiconductors Physics and Materials Properties. Springer, 2010.
3. “Quantum Dots : a True ‘Particle in a Box’ System.” PhysicsOpenLab, 20 Nov. 2015, physicsopenlab.org/2015/11/20/quantum-dots-a-true-particle-in-a-box-system/
4. Cutler, Melvin, and N. F. Mott. “Observation of Anderson Localization in an Electron Gas.” Physical Review, vol. 181, no. 3, 1969, pp. 1336–1340., https://doi.org/10.1103/physrev.181.1336
5. Ramirez, H. Y., et al. “Optical Fine Structures of Highly Quantized InGaAs/GaAs SelfAssembled Quantum Dots.” Physical Review B, vol. 81, no. 24, 2010, https://doi.org/10.1103/physrevb.81.245324
6. “History of Quantum Dots.” Nexdot, 6 Aug. 2018, nexdot.fr/en/history-of-quantumdots/#:~:text=Alexei%20Ekimov%2C%20the%20first%20discovery,in%20a%20molten %20glass%20matrix.
7. “Quantum Dots.” Sigma, 2021, www.sigmaaldrich.com/technicaldocuments/articles/materials-science/nanomaterials/quantum-dots.html
8. Pan, Dengyu, et al. “Hydrothermal Route for Cutting Graphene Sheets into BlueLuminescent Graphene Quantum Dots.” Advanced Materials, vol. 22, no. 6, 2010, pp. 734–738., https://doi.org/10.1002/adma.200902825
9. Quantum Dots – Wissensplattform Nanopartikel.info, 2021, nanopartikel.info/en/knowledge/materials/quantumdots/#:~:text=The%20most%20prominent%20representatives%20of,a%20material%20in%20quantum%20dots.
10. Yadav, Varnika, et al. “2D MoS2-Based Nanomaterials for Therapeutic, Bioimaging, and Biosensing Applications.” Small, vol. 15, no. 1, 2018, p. 1803706., https://doi.org/10.1002/smll.201803706
11. Hasan, Md. Tanvir, et al. “Multi-Drug/Gene NASH Therapy Delivery and Selective Hyperspectral NIR Imaging Using Chirality-Sorted Single-Walled Carbon Nanotubes.” Cancers, vol. 11, no. 8, 2019, p. 1175., https://doi.org/10.3390/cancers11081175

12. Peng, Fei, et al. “Silicon Nanomaterials Platform for Bioimaging, Biosensing, and Cancer Therapy.” Accounts of Chemical Research, vol. 47, no. 2, 2014, pp. 612–623., https://doi.org/10.1021/ar400221g
13. Chen, Xianfeng, and Wenjun Zhang. “Diamond Nanostructures for Drug Delivery, Bioimaging, and Biosensing.” Chemical Society Reviews, vol. 46, no. 3, 2017, pp. 734– 760., doi:10.1039/c6cs00109b.
14. Hasan, Md Tanvir, et al. “Near-Infrared Emitting Graphene Quantum Dots Synthesized from Reduced Graphene Oxide for in Vitro/in Vivo/Ex Vivo Bioimaging Applications.” 2D Materials, vol. 8, no. 3, 2021, p. 035013., https://doi.org/10.1088/20531583/abe4e3
15. Boghossian, Ardemis A., et al. “Near-Infrared Fluorescent Sensors Based on SingleWalled Carbon Nanotubes for Life Sciences Applications.” ChemSusChem, vol. 4, no. 7, 2011, pp. 848–863., https://doi.org/10.1002/cssc.201100070
16. Lin, Ching-Wei, et al. “Spectral Triangulation: a 3D Method for Locating Single-Walled Carbon Nanotubes in Vivo.” Nanoscale, vol. 8, no. 19, 2016, pp. 10348–10357., https://doi.org/10.1039/c6nr01376g
17. Kellum, John A. “Determinants of Blood PH in Health and Disease.” Critical Care, vol. 4, no. 1, 2000, p. 6., https://doi.org/10.1186/cc644
18. Piasentin, Nicola, et al. “The Control of Acidity in Tumor Cells: a Biophysical Model.” 2020, https://doi.org/10.1101/2020.03.22.002113
19. Swietach, Pawel, et al. “The Chemistry, Physiology and Pathology of PH in Cancer.” Philosophical Transactions of the Royal Society B: Biological Sciences, vol. 369, no. 1638, 2014, p. 20130099., https://doi.org/10.1098/rstb.2013.0099